INVESTIGATION OF FLUIDIZED BED BEHAVIOUR USING ELECTRICAL CAPACITANCE TOMOGRAPHY

Abdelwahid Azzi[1], Hiba Bouyahiaoui[1], Abdallah Sofiane Berrouk[2], Andrew Hunt[3], Ian S. Lowndes[4]*

[1]University of Sciences and Technology Houari Boumedien, LTPMP/FGMGP, BP 32 El-Alia, Bab Ezzouar, Algiers 16111, Algeria

[2]Department of Mechanical Engineering, Khalifa University of Science and Technology, Petroleum Institute, PO Box 2533, Abu Dhabi, UAE

[3]Atout Process Ltd, Ardearn, Wilverley Road, New Milton, Hampshire BH25 5TX, U.K.

[4]Process and Environmental Research Division, Faculty of Engineering, University of Nottingham, Nottingham, NG7 2RD, UK

*Corresponding author. Abdelwahid AZZI Tel.: +213 (0) 771 45 89 26.

E-mail address: aazzi@usthb.dz

ABSTRACT

The temporal and cross-sectional distributions of particles in a 127 mm diameter fluidized bed have been obtained using a new generation, high-speed Electrical Capacitance Tomography. Two planes of eight electrodes were used and mounted at 160 and 660 mm from the gas distributor which was a 3 mm thick porous plastic plate made (maximum pore size of 50-70μm). 3 mm diameter, nearly-spherical polyethylene granules made up the bed. Experiments at sampling frequencies of 200-2000 cross-sections per second and gas superficial velocities from just below the minimum fluidization to 83% above minimum fluidization velocities were used. The time series of the cross-sectional average void fractions have been examined both directly and in amplitude and frequency space. The last two used Probability Density Functions and Power Spectral Densities. The information generated show that the fluidized bed is operating in the slugging mode, not surprising given the size of the particles. It has been found that an increase of the excess gas velocity above the minimum fluidization velocity resulted in the increase of the mean void fraction, length and velocity of the slug bubbles as well as the bed height, and in a slight decrease of the slug frequency. The results are presented in a level of detail suitable for comparison with later numerical simulation.

Keywords: Fluidized Bed, Slugging Regime, Void Fraction, Minimum Fluidization, Electrical Capacitance Tomography

1. INTRODUCTION

Fluidization is a process of liquefying a system of solid particles using an intimate contact with a gas or liquid. In doing so, solids acquire a fluid-like behavior that makes fluidized beds the best candidate for many industrial operations. Indeed, fluidized beds have some useful and rather unusual rheological properties with far-reaching consequences on their performance as chemical and physical reactors. As compared to other methods of fluid-solid contacting, fluidized beds are known for their continuous easy-to-handle automatically-controlled operations, [1, 2]. The latter are also simple and reliable, in the case of fluidized beds, owing to the rapid mixing of solids and prevailing nearly-isothermal conditions, [3, 4]. This makes fluidized beds well suited for large-scale operations. Gas fluidized bed applications, potential or established, are inexhaustible. They cover physical operations such as transportation, mixing of fine powders, heat exchange, a coating of plastics on metals, drying and sizing, particle growth and condensation of sublimable materials, and adsorption. As chemical reactors, gas-fluidized beds have been widely used for the high level of mixing that promotes rapid transfer of heat and mass throughout the reactors. Applications such as fluid catalytic cracking and reforming, fluid coking, thermal cracking, carbonization of oil shale and coal, gasification of coal and coke, calcination of limestone and dolomite, cement clinker, roasting of sulfide ores, reduction of iron oxide, oxidation of ethylene, and Fisher-Tropsch synthesis would not exist or have met the current commercial success if they did not tap into the fluidized beds potential to efficiently host such world-changing chemical reactions

A major problem with fluidized beds is the prediction of their behavior under a wide range of operating conditions, [5-7]. This stems from the lack of an accurate description of real contacting patterns within them. Consequently, the development of satisfactory methods for predicting and measuring contacting patterns is crucial to take advantage of this unique behavior offered by

fluidized beds and put it to good use. Without this knowledge, the design of potential new applications will remain an engineering task riddled with uncertainties and therefore unattractive for large investments.

There has been a wide body of theoretical and experimental research dedicated to the study of fluidization and its application for the design of physical and chemical reactors. Hundreds of correlations have appeared in the literature that link fluidized beds most important parameters to their dynamic behavior and how heat and mass are transferred as a result of gas-particle dynamics, [8-10]. Correlations on, for instance, minimum fluidization velocity, minimum bubbling and slugging velocities, bed expansion, and bubble size and velocity have been developed for a wide range of flow conditions, for both spherical and non-spherical particles, for monodispersed and binary systems, and for bubbling and non-bubbling beds fluidized by gas or liquid. Different gas fluidization regimes have also been mapped out as a function of the fluidizing gas velocity. They consist of bubbling, slugging, turbulent, fast fluidization and pneumatic transport cited in the order of increasing gas velocity. Every regime has its own gas and solids dynamics characteristics that decide on its suitability for the such or such process. This suitability also depends on the powder used. For this reason, a classification of the behavior of different types of fluidized powders was developed (A-B-C-D Geldart classification) to give fluidized beds designers the possibility to extend the properties observed for one powder to all powders in the same group without resorting to additional experimental work, [11]. Demarcation criteria between these groups of powders have been also proposed [12-15]. This classification that has been the subject of a constant refinement is based on the properties of the powder such as size, density, fine content, and cohesiveness. These properties play an important role in the calculation and prediction of dynamic behavior in fluidized

beds and the predictive quality of the developed correlations and classification hang much on the accurate estimation of these fundamental parameters.

New technologies have been evolving at a rapid pace offering a convincing set of experimental techniques and protocols [2, 10] that should help researchers and designers improve the accuracy of fluidized beds' behavior description. In particular Electrical Capacitance Tomography (ECT) has proved accurate and adaptable for monitoring particulate flows [16]. In this work, ECT has been shown to provide measurements of concentration distribution, velocity profile and mass flowrate. In addition, the technique is non-invasive, uses no electromagnetic or nuclear radiation and provides fast imaging at up to 5000 frames per second. The sensors can be integrated into high pressure and high-temperature systems (up to 90 bar and 300C) and can even be externally clamped on to both low pressure and high-pressure piping, including under-water [17]. ECT was initially developed at UMIST in the late 1980's, largely under the impetus of Professor Maurice Beck. ECT sensors are made by mounting a series of electrodes around the outside of the flow of interest. The value of capacitance between all pairs of electrodes is measured and the resulting matrix of measurements interpreted through the use of a sensitivity map to give an image or tomograph, typically representing a two-dimensional slice through a vessel. The reconstruction of images is an under-determined inverse problem, but techniques for reconstruction are many and well-developed [18].

Earlier work in the 1970s, work on a capacitance measuring system was initiated at the Morgantown Energy Technology Center (METC) to measure levels of beds, solid flowrates, and gas-solid mixtures parameters [19]. This work led to a non-intrusive system allowing three-dimensional imaging of the voidage distribution in fluidized beds at rates of 60 to 100 frames per second. Halow et al. [19] reported observations of the flow in a fluidized bed using (193 pixels)

resolution system. The bed was imaged in zone 1.25 to 2 bed diameters above the grid, at a rate of 62.5 frames per second for a period of 5.23 s. Imaging was performed [20] in a region 3 to 3.75 bed diameters above the grid, at a rates of 62.5 frames per second for a period of 20.9 s.

The ECT technique has been used to analyze the flow patterns in fluidized beds including those close to the air distributor[21, 22]. Imaging at a frame rate of 210 Hz and 812-pixel resolution was achieved. The results presented concerned three flow regimes: bubbling fluidization, slugging and transition from slugging to a turbulent regime. In other work, the chaos in fluidization was analyzed using ECT to measure the local porosity of gas-solids fluidized bed as well as its time fluctuations [23]. The authors noticed that the METC-type sensor gave reliable results on large scale (28.4 cm diameter) fluidized beds. The effect of pressure on the behavior of fluidized beds of two materials – FCC catalyst (77µm, Geldart type A) and silica sand (203 µm, Geldart type B) was studied using ECT in [24]. Little effect of pressure on the minimum fluidization velocity was found. Using sand as the bed solids, the void fraction increased linearly with gas superficial velocity and the characteristic frequency of the fluctuations in void fraction were seen to be almost independent of gas superficial velocity. The trends for the FCC catalyst were found to be more complex. The technique has been used by other groups prominent in the field [25].

2. CHARACTERIZATION OF SLUG FLOW IN FLUIDIZED BED

If a bed of particles, held initially at the onset of fluidisation, sees its gas velocity gradually increased, bubbles of gas appear and flow upward through the bed while growing in size. By further increasing the gas velocity, the average bubble size increases and may reach the bed characteristic length. At this point, the slugging flow regime is obtained. This intermittent regime consists of successive large bubbles of gas called generally slug bubbles or slugs, followed by

solids plugs. This regime characterizes many important applications taking place within fluidized bed reactors such as polymerization, coal gasification, and catalyst regeneration to name only few. In order to improve the efficiency of such energy-extensive processes, the slug flow behavior should be well quantified through accurate estimation of its important parameters such as slug bubble velocity, frequency, length, bed expansion, and void fraction distribution. These parameters are known for their direct effect on the above-mentioned processes' performance in terms of product yield, selectivity, energy consumption, and operation stability. Many ETC-based investigations of slug flow regime have appeared over the last decade with the purpose to advance our understanding of such flow regime.

Studies of fluctuations caused by bubbles or slugging in fluidized beds have been studied by examining the fluctuation of pressure in the bed [26-28]. More recently, more advanced techniques such as ECT and ultra-fast MRI have also been employed [29, 30]. Reviews are presented on previous work on the velocities [29] and frequencies [30] of the bubbles. Stewart and Davidson [31] proposed that the rise velocity of an axisymmetric slug bubble in a gas-fluidized bed could be described by $0.35\sqrt{(gD)}$where D is the column diameter and g is the gravitational acceleration. This applies when the bubble has the usual bubble shaped nose. When the nose is more square shaped, a values of 0.18 was proposed for the numerical constant. Muller et al. [29] note that it is generally accepted that, for continuously formed axisymmetric bubbles, the excess gas velocity should be added to the single bubble rise velocity. Indeed, they present a general equation

$$u_{sl} = k_1\sqrt{(gD)} + k_2(u - u_{mf}) \qquad (1)$$

with u_{sl} , u , u_{mf} the slug bubble, gas and minimum fluidized velocity respectively; k_1 and k_2 constants determined experimentally.

With regards to frequency of bubbles or slug bubbles, a recent paper [30] cites 9 equations for the prediction of this parameter of which 3 are specifically for slugging beds. For example, Verloop and Heertjes [27] suggested a model which considers a single slug bubble in the bed at any one time and visualizes the cycles that occur as having two parts. One is the rising of the slug through the bed. The other is the bursting of the bubble through the top surface and subsequent rain down of particles thrown up. The time for the second part is assumed much smaller than the first. It was indicated that, to a first approximation, the frequency is $f = u_{sl}/H_M$, where f is the frequency, u_{sl} is the slug rise velocity and H_M is the maximum height of the bed. Assuming that the gas flow out of the top of the slug is given by u_{mf}, the height increase is taken to be caused by the inflow of gas during the slug rise. This results in

$$H/H_{mf} = u_{sl}/(u_{sl} - u_{mf}) \qquad (2)$$

Using equation (1) with $k_1 = 0.35$ and $k_2 = 1$ results in

$$f = 0.35\sqrt{gD}/H_{mf} \qquad (3)$$

Baeyens and Geldart [26] followed a similar approach. They defined the length of the slug as h_s and that of the wake (the bed between slugs) as W_s. Frequency is given by $f = u_{sl}/(W_s + h_s)$. A mass balance over the slug and wake resulted in $h_s/(W_s + h_s) = (u - u_{mf})/u_{sl}$. Which substituted in the definition of frequency gives $f = (u - u_{mf})/h_s$. The total heights of n wakes and n slugs are $nW_S = H_{mf}$ and $nh_s = H - H_{mf}$ respectively. It can be shown that $(u - u_{mf})/u_B = (H - H_0)/H_0$, where H is the total height of the slugging bed and H_{mf} is the height at minimum fluidization. u_B is the rise velocity of a single slug for which Baeyens and Geldart took the Stewart and Davidson [31] relationship. Combining these yields

$$h_s = (u - u_{mf})k\sqrt{D}/(0.35\sqrt{g}) \qquad (4)$$

where k is the ratio of wake length and bed diameter. Substituting into the definition of frequency yields:

$$f = 0.35\sqrt{g}/k\sqrt{D} \qquad (5)$$

For deeper beds, this reduces to $f = 0.61D^{-0.143}$. Note the constant differs from that in the Baeyens and Geldart paper [26] as here D is in meters not centimeters.

Recently, beds fluidizing Geldart-D-type particles have been investigated using two-plane electrical capacitance tomography (ECT) sensors in order to determine the onset of fluidized bed regimes [32]. Computation and analysis of standard deviations of the solids fraction recorded at each plane of the ECT sensor for different superficial gas velocities are conducted. The results show that the onset of slugging is recorded at the peak of the difference in the solids fraction fluctuation between the two planes.

The present paper investigates the behavior of a fluidized bed gasifier using the ECT technique. It reports on our commissioning work which has used larger polyethylene pellets (3 mm) rather than the finer pulverized coal (60 μm) more commonly used in the gasifiers. Results on the slugging flow dynamics that generally characterised the fluidization of Geldart D type particles are presented and analyzed based on information extracted for slugs' lengths, frequencies, and velocities. The method developed in this study provides a means of obtaining an accurate account on the onset of slugging in fluidized beds.

3. EXPERIMENTAL FACILITY

A schematic diagram of the fluidization rig, built at the Chemical and Environmental Engineering Department of the University of Nottingham, UK, to carry out the present experiments, is shown in Figure 1.

The flows were established in a 4m long vertical pipe of 127 mm internal diameter made up of transparent acrylic resin pipe. The pipe is filled with the bed granular material (in this case polyethylene - granules of nearly spherical shape approximately 3mm in diameter) and the air is introduced from the laboratory supply through an air distributor which consists of a 3 mm thick porous plate made of plastic with a maximum porous size of 50-70 μm. Below the air injector, there is a conical section filled with 6 mm diameter glass beads to create an even distribution of the flow. The air flow rate is measured using a calibrated variable area meter. The bed material has a density of 915 kg m^{-3} and a bulk density of 558 kg m^{-3} which corresponds to an as-poured void fraction of 0.39. These particles are class D in the classification proposed by Geldart [11] as shown in Figure 2.

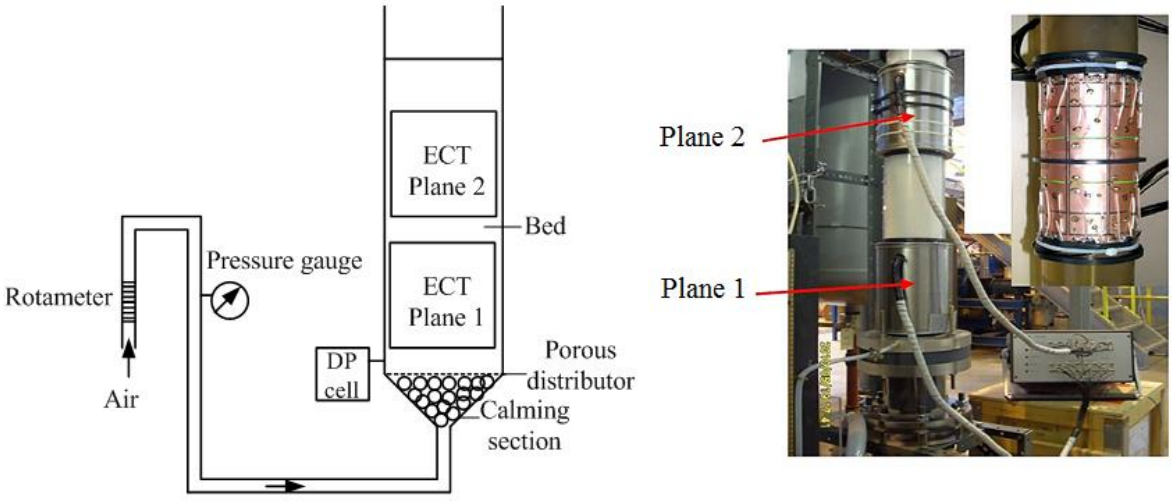

Figure 1. Schematic and photographs of fluidization rig and probes showing electrodes (top right) which are screened in use (left of photograph).

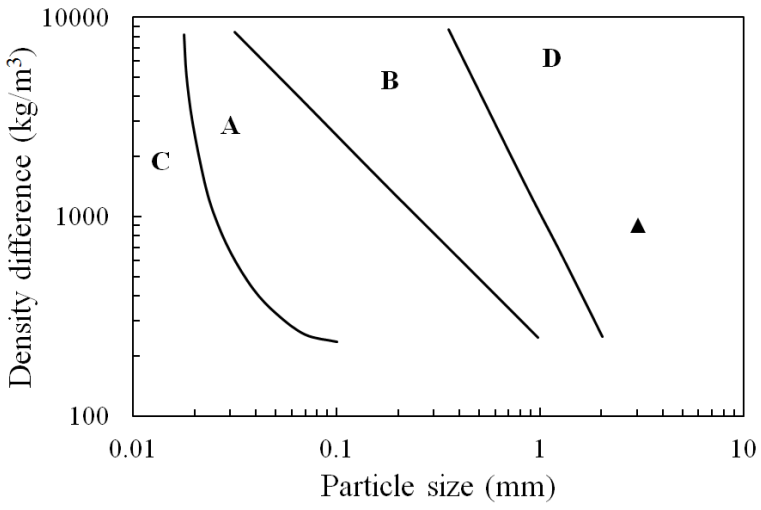

Figure 2. Geldart map [11] and the present particles

4. ELECTRICAL CAPACITANCE TOMOGRAPHY INSTRUMENTATION

The Tomoflow R5000 high-speed imaging system was used for imaging concentration and measuring velocity in the fluidized bed. Data can be captured at rates up to 5000 image frames per second, but in the experiments reported here, the frame rate was between 200 and 2000 cross-sections per second. The measurement noise level at 500 fps was typically 0.02fF rms and the range of capacitance in the 28 independent pairs of electrodes was between 10fF (across the pipe) and 300fF (adjacent electrodes).

The sensor was assembled as two separate planes of measurement electrodes, each containing a full set of driven guard electrodes running axially before, between and after the measurement planes ensuring that an axially-uniform electric field was maintained over the capacitance sensor cross-section. The measurement system can drive the two sets of guards and the two measurement

planes independently through a total of 32 co-axial connections, enabling the sensor planes to be spaced at different separations

Measurements were made between all pairs of electrodes within each plane around the sensor using a charge/discharge capacitance technique. An excitation signal was used in the form of a 15V peak to peak square wave with a frequency of 5 MHz.

Inversion of the 28 capacitance pairs to an 812-pixel image on a 32x32 square grid was undertaken using a technique known as linear back projection, and component information (void fraction etc.) is extracted from these images. Cross-correlation between the image planes gives the velocity distribution across the flow. The two electrode rings were positioned with their centrelines 160 and 660 mm from the distributor plate while the physical length of each measurement electrode is approximately 50% of the bed diameter and the overall guarded length exceeds the bed diameter. The two planes were mounted at 160 and 660 mm from the gas distributor.

ECT generates images, typically shown as a 32x32 pixelated map of the pipe cross-section, often circular. The details of these depend on the physical parameter being displayed, the assumptions made in the physical modeling, and the color scale.

For any electrical measurement, including ECT, the choice of a physical model linking the measured permittivity to concentration is critical. The capacitance measurement in ECT is converted to electrical permittivity from calibration. To move from this electrical measurement to a fluid-mechanically useful measure of concentration involves the use of a physical model linking the two. The expression used in [16] as the 'Maxwell' model applies to non-conducting spheres distributed uniformly in a non-conducting medium.

$$\varepsilon_m = \varepsilon_1\left[1 + 3v(\varepsilon_2 - \varepsilon_1)/\left(\varepsilon_2 + 2\varepsilon_1 - v(\varepsilon_2 - \varepsilon_1)\right)\right] \qquad (6)$$

where ε_m is the effective mixture permittivity of a distribution of spherical particles, ε_1 is the material permittivity of the continuous medium, ε_2 is the material permittivity of the spherical particles, and v is the volumetric fraction of space occupied by the spheres (referred to here as void fraction).

Given the wide range of distributions of gas, any measurement technique that has an average across the flow as primary output will be subject to substantial errors due to the sensor sensitivity distribution – in the case of a gamma-ray densitometer a single line average for example. The great advantage of ECT (and other imaging techniques) is that the reconstruction process accounts directly for the sensor sensitivity and creates a corrected distribution. The average of the pixelated data is, therefore, an accurate measurement of the mean void fraction whatever the gas distribution.[16]

5. RESULTS AND DISCUSSION

The minimum fluidization velocity was determined to be 0.79 m/s from a plot of pressure drop across the bed against the gas superficial velocity (Fig.3). Graphically, the minimum fluidization velocity is the point of intersection between the two straight lines on the plot of bed pressure drop vs. gas velocity. This compares well with values calculated from correlations in the literature (within 15%), Hilal et al. [33]

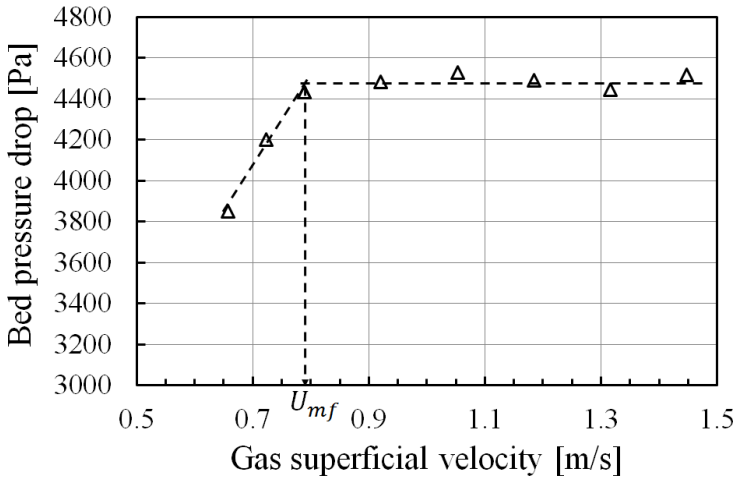

Figure 3. Bed pressure drop vs. gas superficial velocity

As the fluidized bed was made from transparent acrylic resin pipe, it was possible to observe visually the bed behavior. Below the minimum fluidization velocity, there is hardly any motion in the bed. However, at higher velocities, there are sudden expansions of the bed with a large plug of particles being pushed upwards. Individual particles rain down from these plugs.

In all the experiments reported here the initial height of the beds was 0.85 m. Measurements were made at eight gas superficial velocities, three below and five above the minimum fluidization velocity. Tests were carried out at sampling frequencies of 200, 1000 and 2000 cross-sections per second.

5.1 ELECTRICAL CAPACITANCE TOMOGRAPHY OUTPUTS

Figure 4(a) shows two ways of looking at the images – the right-hand side of the figure shows the cross-section of the flow, while the left-hand side shows a projection of the horizontal centre line of pixels stacked against time, with time increasing from the top – this gives the impression of a vertical 'slice' through the flow. It can be seen that the gas is predominantly off-centered to the

right of the images at this experimental time. Figure 4(b) shows the same type of images for the higher plane of electrodes (plane 2) where the bed has a large slug bubble present. Both Figure 3(a) and Figure 4(b) are at an excess velocity of 0.0m/s, the onset of fluidisation.

Figure 4(c) to Figure 4(h) show representative cross-sectional images at certain key times to illustrate the different flow conditions observed. Excess velocity increases from Figure 4(c) to Figure 4(h) as shown in the caption from 0.0 m/s to 0.66 m/s. For each velocity the bottom two images show the distribution of solids and gas in plane 1, the lower plane of electrodes, while the upper two images show the distribution of solids and gas in plane 2, the upper plane of electrodes. On the left of each of Figures 4(c) to Figure 4(h) the two images are at the time indicated above them, when the void fraction in plane 1 is a maximum, while the right-hand stack of 2 images are taken at a time when the void fraction in plane 2 is a maximum. Figure 4(c) shows bubbling in plane 1 and slugging in plane 2, Figure 4(d) shows large bubbles in both planes with solids falling through the centre and edge of the cross-section, Figure 4(e) shows large slug bubbles passing up one side of the bed, Figure 4(f) to Figure 4(h) show the slug bubbles tending to become annular or occupying the entire cross-section.

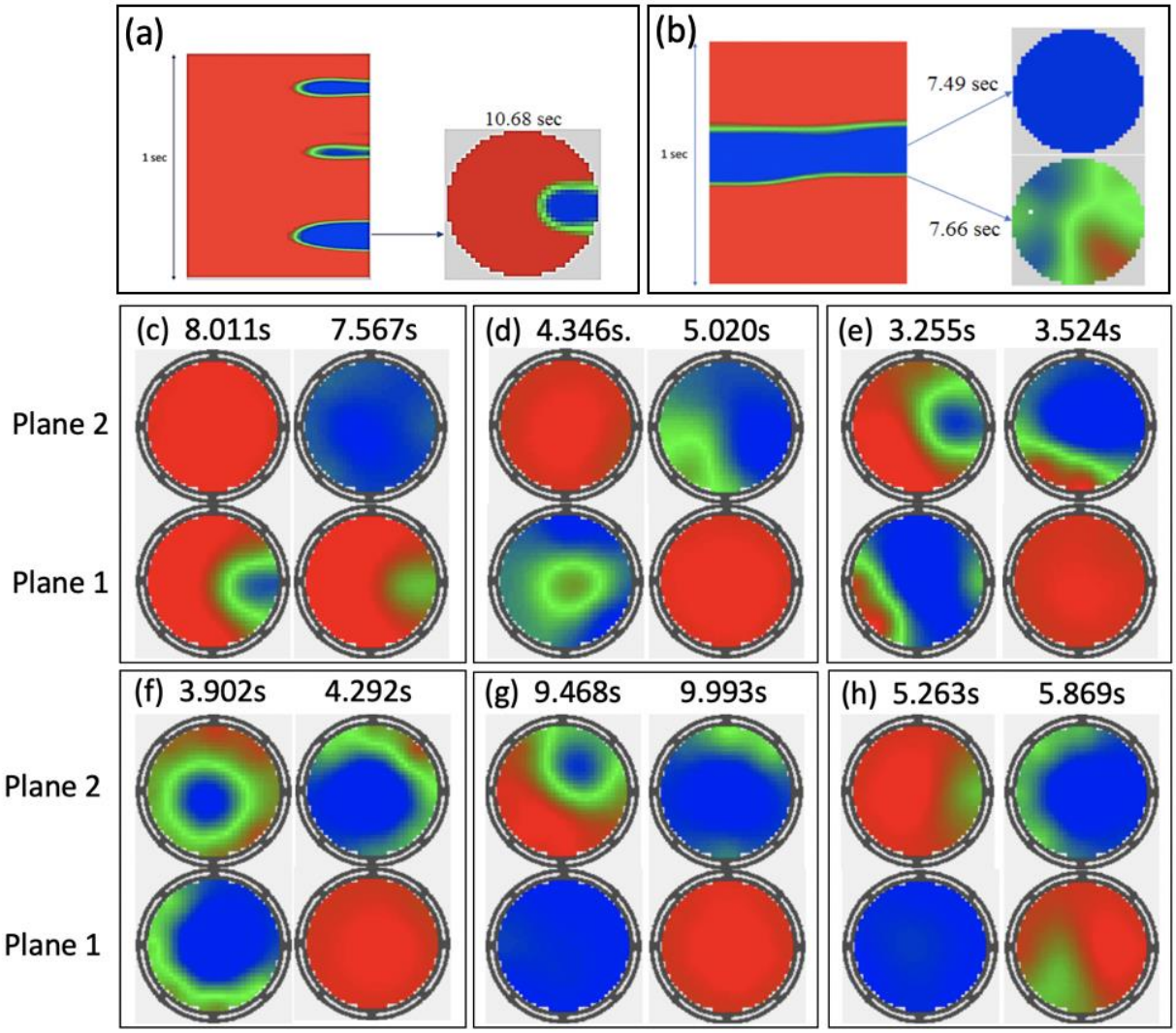

Figure 4. Images generated from ECT data at sampling frequency = 1000 Hz : (a) plane 1 LHS vertical 'slice' of 1 second, RHS single cross-section, (b) plane 2 – LHS vertical 'slice' of 1 second, RHS single cross-section, (c) excess gas velocity above minimum fluidization 0.0 m/s, (d) 0.13 m/s, (e) 0.26 m/s, (f) 0.39 m/s (g) 0.52 m/s, (h) 0.66 m/s. RGB colour scale where red = packed bed, blue = gas, green = intermediate concentration of solids.

5.2 TIME SERIES OF CROSS-SECTIONAL AVERAGE VOID FRACTION

The output of the Electrical Capacitance Tomography can be examined at several levels. The simplest is to obtain time series of the cross-sectionally averaged void fraction. Examples of these are shown in Figures 5 to 10. From Figure 5; for which the gas velocity is just above the minimum fluidization velocity, u_{mf}, there are only very small fluctuations at the lower plane with evidence of small bubbles at the upper plane. Increasing the gas flow rate until the velocity is 0.13 m/s above u_{mf}, there is evidence of small bubbles at plane one with fully developed slug bubbles, where there are hardly any particles present in the cross section at plane 2 as illustrated in Figure 6. Further increasing the gas velocity to 0.26 m/s above the u_{mf}, shows a combination, of slug bubbles and small bubbles at the lower plane and slug bubbles at the top plane, Figure 7. For 0.39 m/s above u_{mf} (Figure 8), illustrates slug bubbles at both planes 1 and 2. Figures 9 and 10, excess velocities of 0.53 and 0.66 m/s illustrate how the slugs are no longer viable near the distributor.

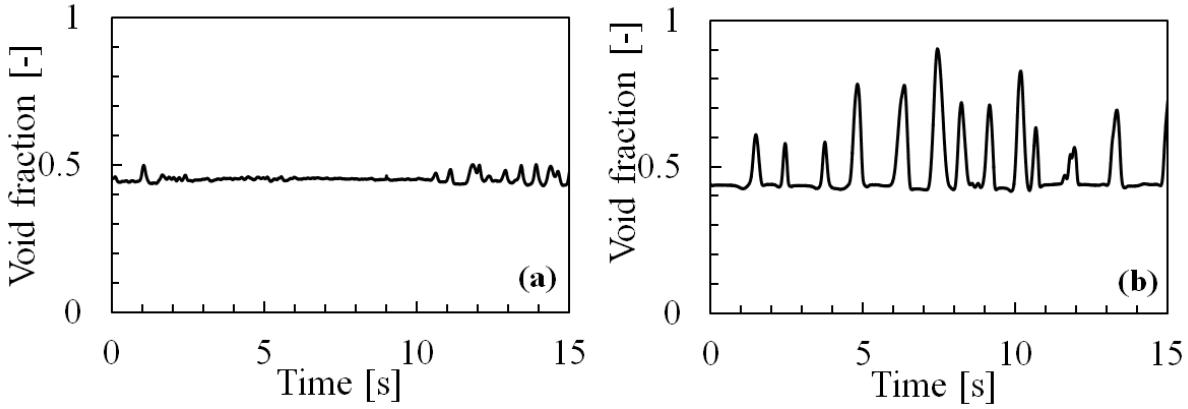

Figure 5. Cross-sectional average void fraction's time series. a) Plane 1, b) Plane 2. Excess gas velocity above minimum fluidization 0 m/s. Sampling frequency = 1000 Hz.

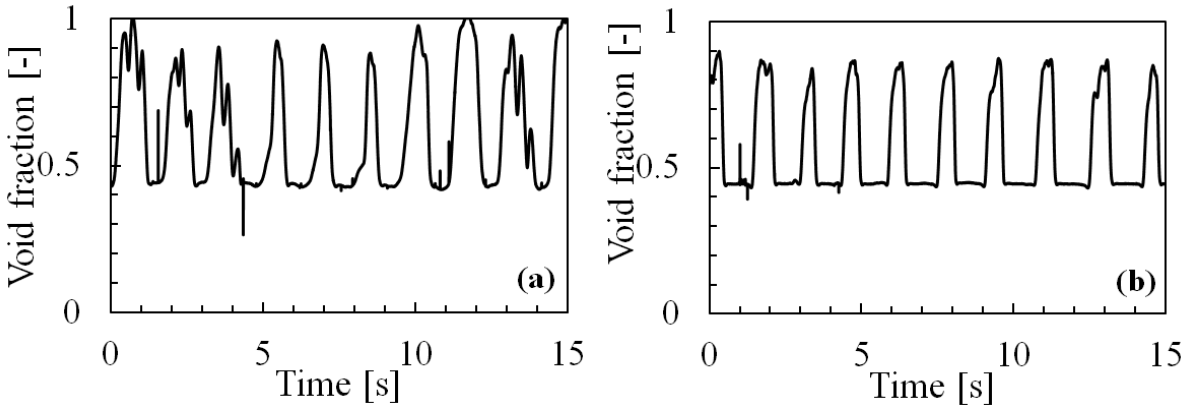

Figure 6. Cross-sectional average void fraction's time series. a) Plane 1, b) Plane 2. Excess gas velocity above minimum fluidization 0.13 m/s. Sampling frequency = 1000 Hz.

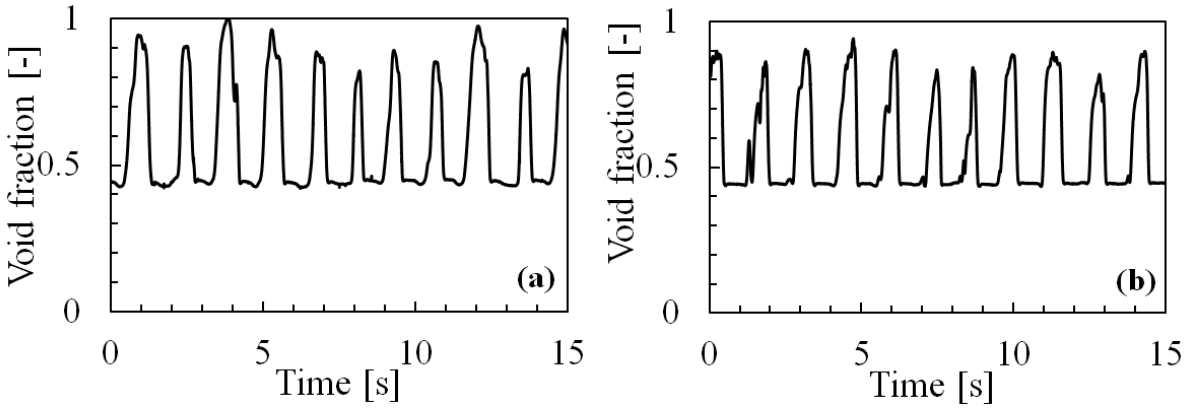

Figure 7. Cross-sectional average void fraction's time series. a) Plane 1, b) Plane 2. Excess gas velocity above minimum fluidization 0.26 m/s. Sampling frequency = 1000 Hz.

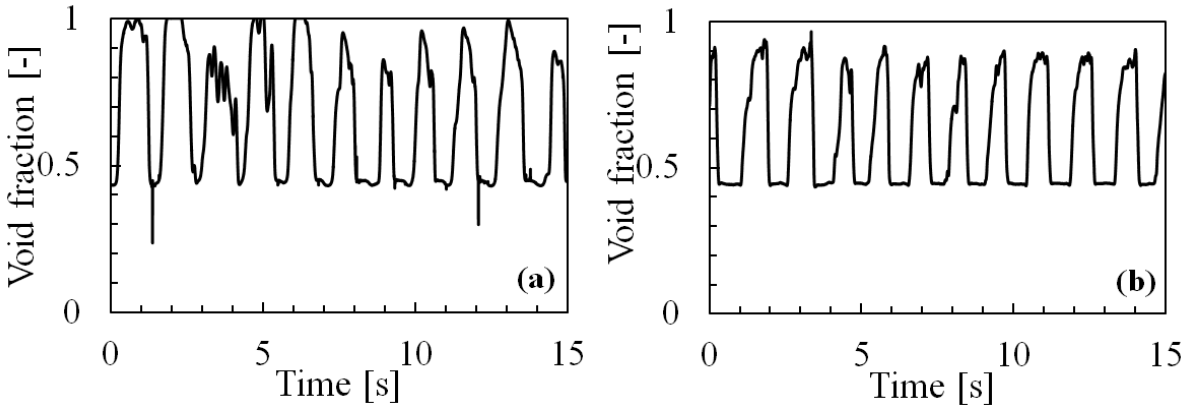

Figure 8. Cross-sectional average void fraction's time series. a) Plane 1, b) Plane 2. Excess gas velocity above minimum fluidization 0.39 m/s. Sampling frequency = 1000 Hz.

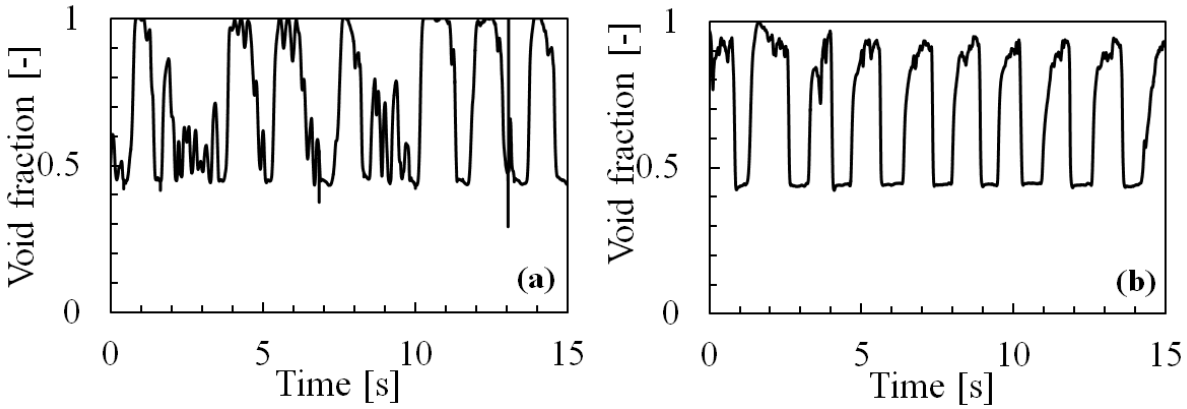

Figure 9. Cross-sectional average void fraction's time series. a) Plane 1, b) Plane 2. Excess gas velocity above minimum fluidization 0.53 m/s. Sampling frequency = 1000 Hz.

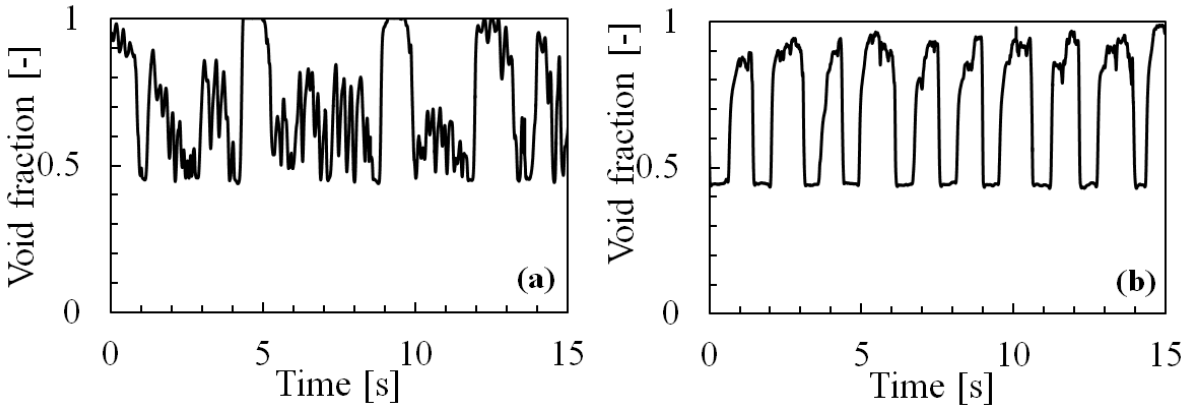

Figure 10. Cross-sectional average void fraction's time series. a) Plane 1, b) Plane 2. Excess gas velocity above minimum fluidization 0.66 m/s. Sampling frequency = 1000 Hz.

It is apparent from Figure 5 to Figure 10 that once slugging becomes established above 0.13 m/s excess velocity, the void fraction in the upper plane (Plane 2) is limited between 0.39 (packed bed) and approximately 0.9 (falling or bypassed solids occupying the remaining 10% or so). Increasing flowrate can therefore only be manifested through increase in slug velocity, length or frequency. The velocity of a slug bubble is limited by the bed diameter, and it is apparent from the graphs of void fraction that the frequency remains fairly constant and it is the slug length that increases, though beyond 0.53 m/s excess velocity there is little obvious change. Referring back to Figure 4, ECT gives us the ability to see that what is happening at the higher velocities is that the slugs are starting to progress towards annular flow where the velocity will not be limited by the pipe diameter in the same way.

5.3 EVOLUTION OF AVERAGE VOID FRACTION WITH GAS VELOCITY

The time-averaged void fractions are illustrated in Figure 11. Figure 11 (a) shows that the sampling rate has only a small effect on the results. Obviously, below the minimum fluidization velocity,

there is hardly any effect of gas flow rate. Beyond this value, the void fraction increases with gas velocity. However, eventually, it plateaus out to a constant value.

The difference in mean void fraction up the bed (between plane 1 and plane 2) can also be examined. Figure 11(b) shows that the general trend is the same but there are fewer fluctuations in plane 2. It is worth noting that the mean void fraction increases with excess gas velocity in the same manner as the mean void fraction with gas superficial velocity in gas-liquid two-phase slug flows as reported by several previous authors such as Azzopardi et al. [34]

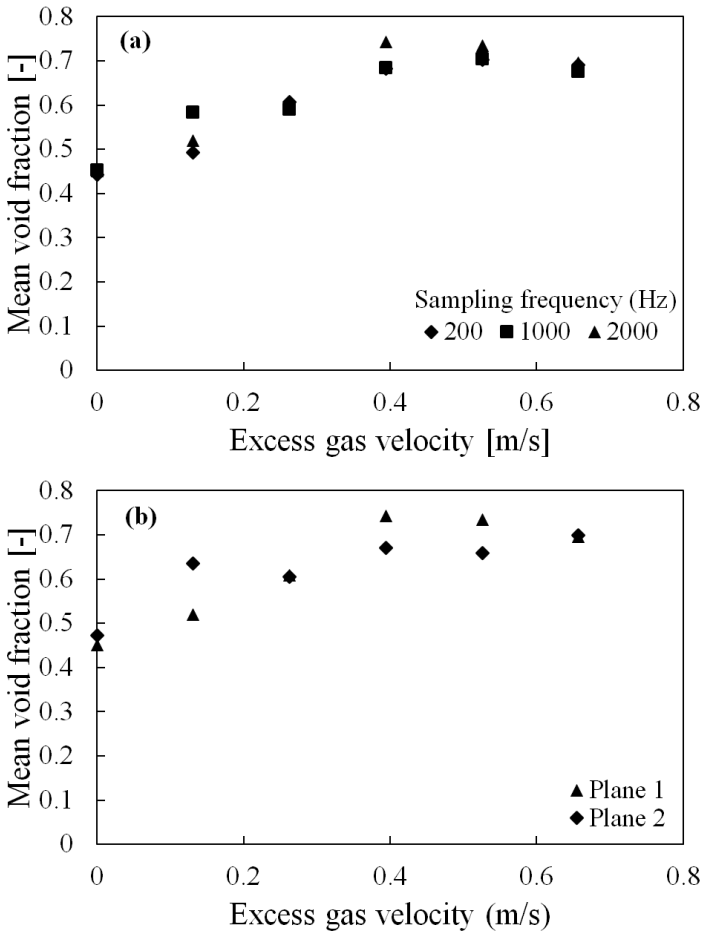

Figure 11. Variation of the void fraction with gas superficial velocity. (a): Effect of sampling rate - Plane 1. (b): Difference between two sampling planes -1000 Hz.

5.4 PDFS OF THE TIME SERIES OF CROSS-SECTIONAL AVERAGE VOID FRACTION

The Probability Density Function PDF of the void fraction represents the rate of change of the probability that void fraction values lie within a certain range versus void fraction. The total area under the probability density function must equal unity. It can be used as a tool for flow regime identification of Costigan and Whalley[35]. The PDF of the bubbly flow shows only one peak, while the slug flow regime shows two distinct peaks. Figure 12 shows the PDFs of the average void fraction time series at plane 1 and 2 for the excess gas velocity above the minimum fluidization velocity from 0 to 0.66 m/s. For excess gas velocity equal to 0 m/s (Figure 12(a)), the PDFs show a single peak for both planes showing that there are only small bubbles in these planes for this flow conditions. An increase of the excess velocity to 0.13 m/s (Figure 12(b)), results in the change of the PDF corresponding to plane 1 with a tail up to high values of void fraction expressing the increase of the void fraction in this plane; while the PDF of the upper plane presents two distinct peaks, one at low value of void fraction and the second one at a high value of void fraction of about 0.85. The form of the PDF at plane 2 confirms the presence of slug flow at this position.

For excess gas velocity of 0.26 m/s (Figure 12(c)), has a consequence of the existence of small bubbles and slug bubbles at the lower plane with a PDF presenting a single peak at a low void fraction and the beginning of the appearance of a second peak at high void fraction value. The PDF of the top plane with two distinct peaks depicts the occurrence of slug flow at this position.

Figure 12(d) for which the excess gas velocity is equal to 0.39 m/s, shows the slug bubbles at both planes with the signature of the PDFs with two distinct peaks.

In Figures 12(e) and 12(f), for which the excess velocities are 0.53 and 0.66 m/s respectively, there is a range of void fractions present at the lower plane. The PDFs exhibit only one peak just above the void fraction equal to 0.4 showing the existence of only small gas bubbles. However, by the higher plane, large bubbles (slug bubbles) have been formed and the flow consists of alternate zones of gas and packed beds; and the PDFs show two distinct peaks, one at low void fraction and one at high void fraction; a classical PDF's signature of a slug flow.

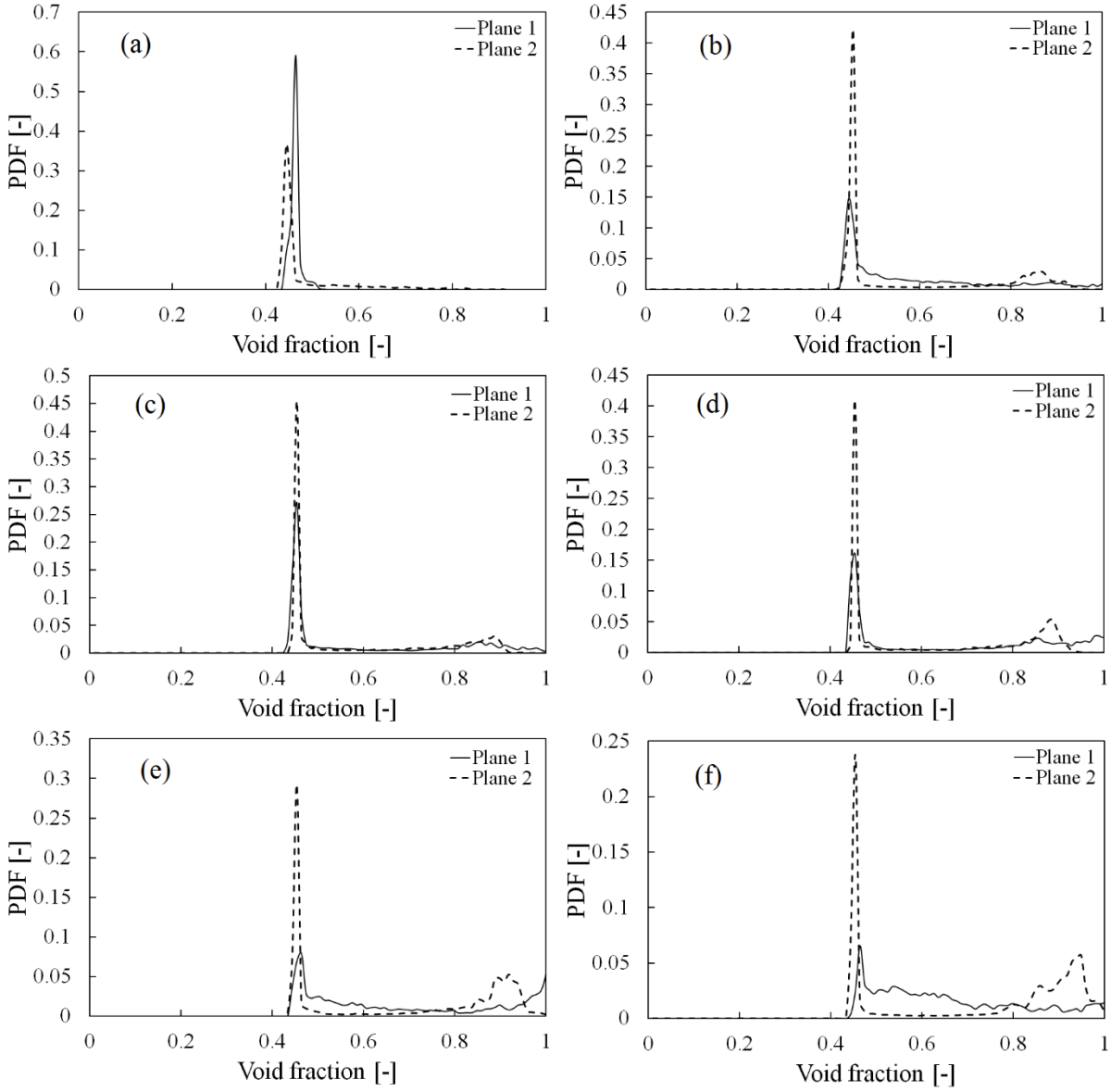

Figure 12. Probability Density Function of the void fraction for the two sampling planes. Excess gas superficial velocity (above the minimum fluidization velocity) = (a) 0 m/s, (b) 0.13 m/s, (c) 0.26 m/s, (d) 0.39 m/s, (e) 0.53 m/s, (f) 0.66 m/s; – sampling rate 1000 Hz

5.5 SLUG BUBBLE VELOCITY

The time series presented in Figures 5 to 10 can be analyzed using a cross-correlation of the signals from the two probes from which the time delay between the two probes and the mean velocity of slug bubbles and solids plugs can be determined. The data can also yield the velocities of individual slug bubbles and solids plugs. Hereafter the method used here to extract graphically these velocities is described. A threshold method was used to discriminate between slug bubbles and solid plugs (Figure 13). A value of 0.5 was set for this threshold. The time delay that takes the slug front to pass from plane 1 to plane 2 refereed by $\Delta t_{Front(i)}$, corresponds to the AB straight segment; and the time delay that takes the slug back to pass from the lower plane to the upper one is refereed by $\Delta t_{Back(i)}$, is the CD straight segment. These time delays are substituted in equations (7) and (8) to determine the velocity of the slug back and front velocity respectively:

$$U_{B(i)} = de/\Delta t_{Back(i)} \qquad (7)$$

$$U_{F(i)} = de/\Delta t_{Front(i)} \qquad (8)$$

where *de* is the distance between the two probes. EF segment represents the time duration of the i[th] bubble slug $\Delta t_{Bubble\ slug(i)}$.

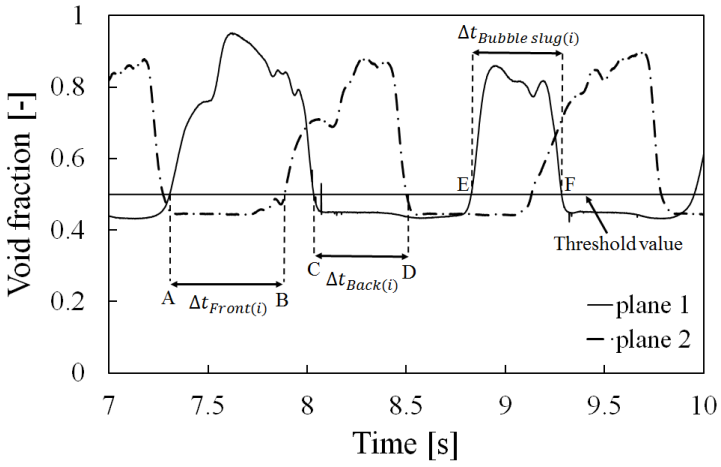

Figure 13. Example of the time delays extraction of the front and back of bubble slug using single threshold technique

The temporal evolution of the front and back velocities of the slug bubbles for four chosen gas velocities using this technique are plotted in Figure 14**.** It is clear from this figure that there is a scatter of individual values and there is no obvious trend with time.

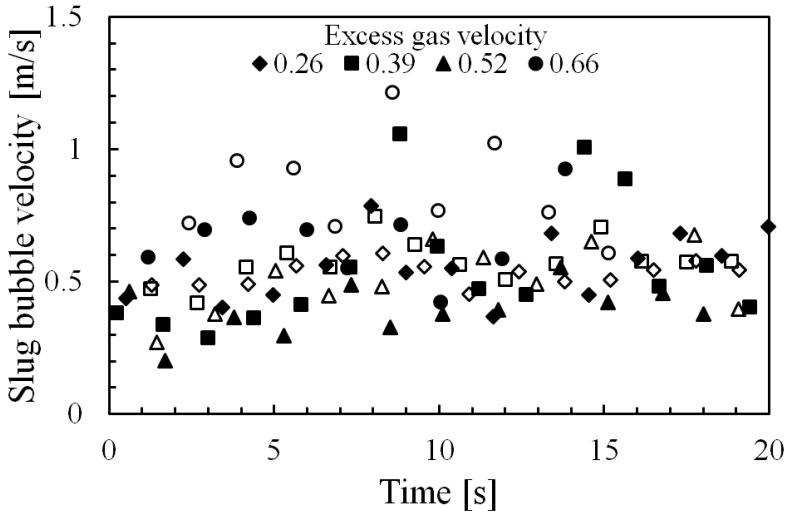

Figure 14 Velocities of front and back of slug bubbles: closed symbols front velocities, open symbols back velocity

The mean values of the velocities of the front and the back of the bubbles plotted in Figure 14 together with those obtained from cross-correlation of the cross-sectional average void fraction's time series between planes 1 and 2 are plotted in Figure 15. Additionally, the curve predictions of these velocities (slug) using the approach of Matsen et al. [36] and Lee et al. [37] by taking the value of k1 and k2 equal to 0.35 and 1; and 0.18 and 0.6 respectively, are plotted in this figure.

As can be seen in Figure 15 there is a wide range of variation in the individual velocities. However, the mean values from these individual velocities are in close agreement with those from the cross-correlation. The values observed here are in the range of the two comparisons [36] and [37] but indicate in the present case very little increase with excess gas velocity.

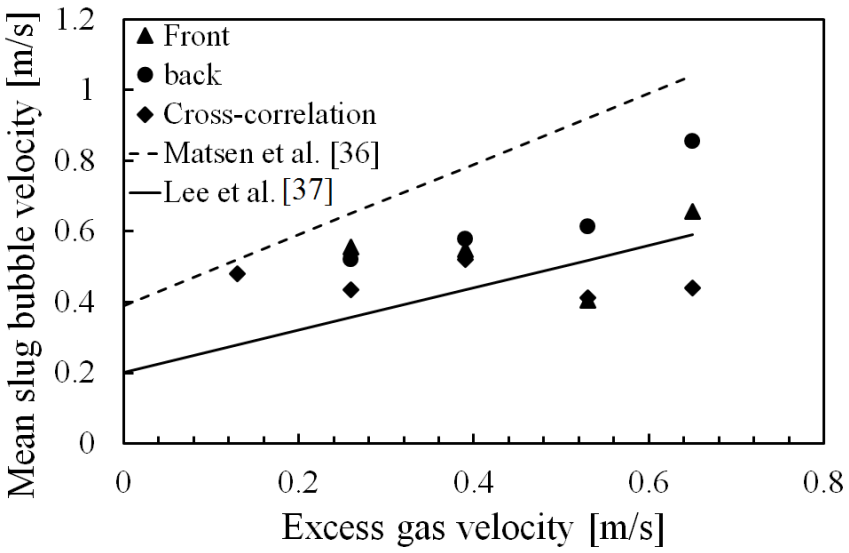

Figure 15 A plot of the computed mean slug bubble velocities as a function of the excess gas velocities employed

5.6 FREQUENCY

Power Spectrum analysis can be used to obtain the frequency characteristics of the times series. Herein, we performed a Fourier transform of the auto-covariance functions to obtain the Power Spectrum Densities (PSD). A discrete cosine transform was applied for the purpose of this analysis since the auto-covariance function does not have a phase lag. For a given signal x(t), the corresponding auto-covariance function is given by the expression:

$$R_{xx}(k\Delta\tau) = \frac{1}{T-\tau}\int_0^{T-\tau}[x(t) - \bar{x}].[x(t + k\Delta\tau - \bar{x}]dt \; ; \tau < T \qquad (9)$$

where $k\Delta\tau$ is the time delay, $\Delta\tau$ is the interrogating time delay, T is the sampling duration, and $\bar{x} = \frac{1}{T}\int_0^T x(t)\, dt$.

The Power Spectrum Density is determined by the equation:

$$P_{xx}(f) = \Delta\tau\left(\frac{1}{2}R_{xx}(0) + \sum_{k=1}^{\tau/\Delta\tau-1} R_{xx}(k\Delta\tau)w(k\Delta\tau)\cos(2\pi f k\Delta\tau)\right) \qquad (10)$$

where $w(k\Delta\tau)$ is a windowing function, is used to remove the spectrum leakage which mainly comes out as the side lobes at the high frequency end of the spectrum. The use of an appropriate windowing function will clearly identify the frequencies contributing to the system. As an initial analysis, a basic cosine windowing function was used,

$$w(k\Delta\tau) = \cos\left(\frac{\pi k\Delta\tau}{2\tau}\right) \qquad (11)$$

Figure 16 shows examples of the Power Spectral Density for void fraction taken at plane 1 for a range of gas velocities. These all show a clear peak, the most likely frequency.

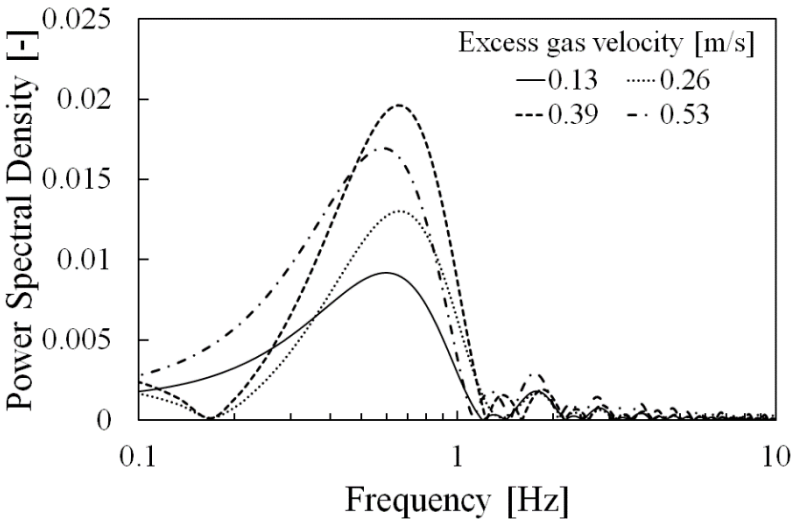

Figure 16. Power Spectral Densities for plane 1 for different excess gas superficial velocity. Sampling frequency = 1000 Hz.

Similar curves are obtained from the data taken at plane 2. Here there is less variation in the position of the peak. The frequency at which the peak occurs can be taken as the most probable frequency. The frequency values obtained for both planes along with those obtained experimentally by Lee et al. [37] and Baker and Geldard [28] are plotted in Figure 17. One can see that for all data, the frequency decreases very slightly with the excess gas velocity increasing. The present values are close to those of Baker and Geldart and lower than those reported by Lee et al. [37]. This is expected as the former performed experiments with plastic beads of 3.8 mm and bed diameter of 150 mm close to the presents experiments while the latter used beads of 1.23 mm and bed diameter of 380 mm.

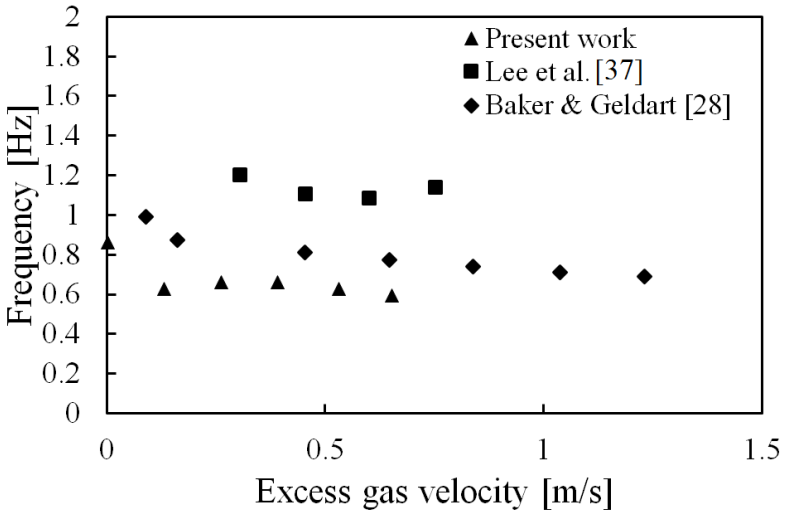

Figure 17. Effect of excess gas on characteristic frequency. Sampling frequency = 1000 Hz.

5.7 SLUG BUBBLE LENGTH

The slug bubble length is defined as the product of the bubble front velocity U_F and the duration of the bubble itself Δt_{Bubble}:

$$L_{Bubble(i)} = U_F \Delta t_{Bubble(i)} \qquad (12)$$

with $\Delta t_{Bubble(i)}$ obtained graphically from Figure 13

Figure 18 shows the temporal variation of the individual slug bubbles length for each fixed excess gas velocity above minimum gas fluidization velocity. It is clear that the slug bubble length increases with excess gas velocity.

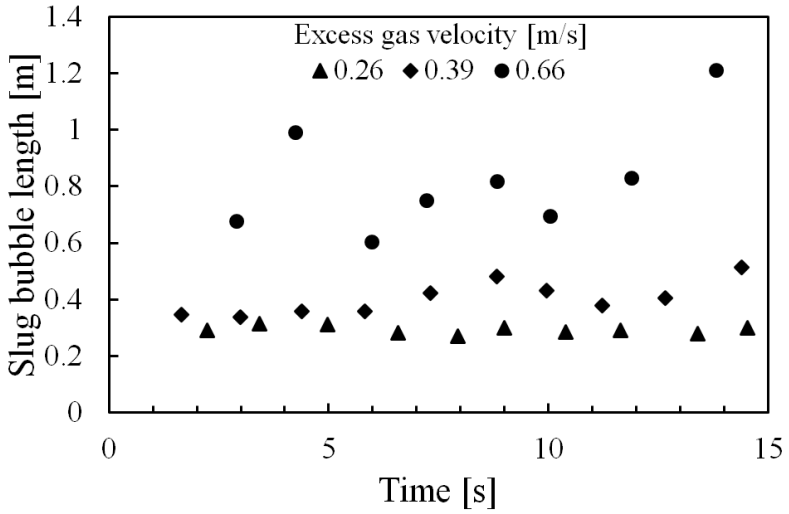

Figure 18 Time series of slug bubble length for each excess gas velocity

It is clear from Figures 15, 17 and 18 that the effect of increasing excess gas velocity is to give longer bubbles at the same frequency with only a slight increase in velocity.

5.8 BED HEIGHT

It appears from figure 18 that the for each excess gas velocity above minimum fluidization velocity, the slug bubble length varies with time. It's obvious that this variation will result in the variation of the bed height. The instantaneous height of the bed can be expressed by the following equation:

$$H(t) = H_0 + 4V_s(t)/\pi D^2 \qquad (13)$$

With H_0 the initial bed height (0.85 m), D diameter of the bed and $V_S(t)$ the instantaneous volume of the slug bubble. The latter is determined accordingly to Matsen et al. [36]:

$$V_S(t) = f(L_S(t)/D)\pi D^3/4 \qquad (14)$$

with:

$$f(L_S(t)/D) = L_S(t)/D - 0.495\ (L_S(t)/D)^{0.5}+0.061 \qquad (15)$$

where $L_S(t)$ represents the instantaneous length of the slug bubble.

The time variation of the bed height obtained using this approach corresponding to each excess gas velocity, are plotted in Figure 19. It is obvious that the bed height increases with excess velocity similarly to the slug bubble. It can reach a height of about three times the initial bed height for the highest excess gas velocity.

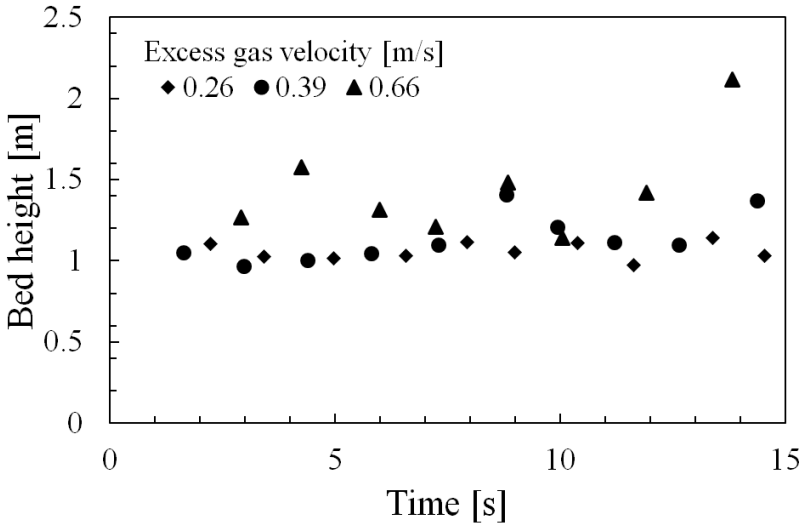

Figure 19 Temporal variation of the bed height function for each excess gas velocity

In order to ascertain our findings that the present data correspond to stable slugging zone, the fluidized bed flow regime classification of Baeyens and Geldart [26] has been used. The authors reported the existence of three distinct zones: freely bubbling (Zone I), slugging with limited coalescence (Zone II) and stable slugging with no further coalescence (Zone III). They formulated the boundaries between these zones by two equations relating the bed height to the diameter of the

bed in cm. In Figure 20, the boundary lines and their corresponding equations as well the average heights obtained for the three excess gas velocities in the present study are shown in Figure 20. It is obvious from this figure that the present data lie primarily in the stable slug region, though the lower velocities are approaching Zone II where some unstable coalescence has been observed near the injector in the lower plane.

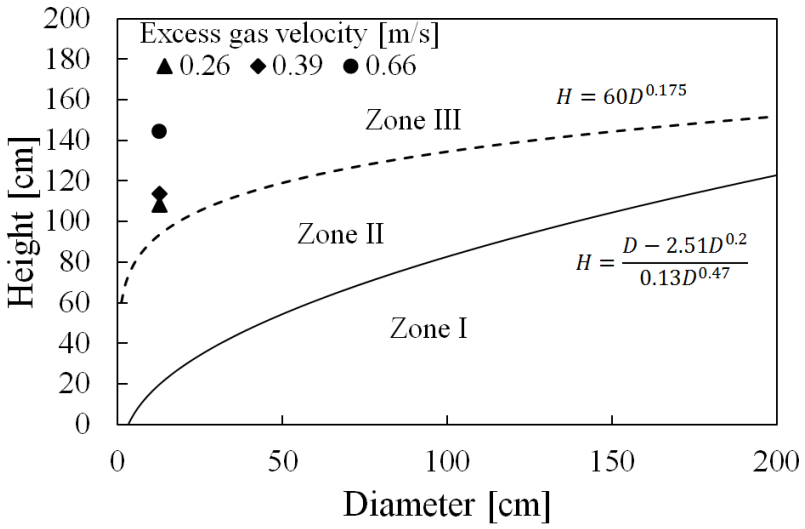

Figure 20 Fluidised bed flow regime zones according to Baeyens and Geldart [26] and the present data

6. CONCLUSION

The results presented herein represent the outcome of the first application of a new generation ECT equipment to Geldart type D particles. From the results presented above, it has been shown that ECT has great capability for interrogating fluidized beds. By examining the void fraction cross-sectional average time series and the detailed cross-sectional images, many features of the flow can be identified such as the slugs' void fraction, velocity and frequency and the lengths of the

slug bubbles and the bed height. More advanced methods for data presentation are illustrated and the extracted slug velocity and frequency data are seen to agree well with predictions from published equations. We note that the main effect of increasing excess gas velocity is to give longer bubbles at the same frequency with only a slight increase in velocity. The results are presented in a level of detail suitable for comparison with later numerical simulation.

The hydrodynamic properties identified here using ECT can be used to optimise design of fluidised bed systems. For example the tendency of the slug bubble to become very long, tending to annular flow above 0.53 m/s shows that the residence time of the gas can be optimised at a lower flowrate, while the cross-section images in Figure 3 can be used to establish optimal mixing patterns for any given design of bed.

This work is restricted to one particle type and size, and one bed diameter. ECT shows no limitations in terms of sampling frequency, but the images have limited spatial resolution where individual particles cannot be seen, though even the concentration of the smallest bubbles and flow structures are accurately captured in the average measurements. The physical length of the measurement electrodes is about half the bed diameter, so that the images are averaged over that length. This effect is minimised by the guarding of the measurement electrodes which minimises any spread of the electric field beyond the measurement electrode length.

REFERENCES

[1] D. Kunii and O. Levenspiel, Fluidization Engineering, 2nd Edition , Butterworth Heinemann, Boston , USA. 1991

[2] W. C. Yang, Handbook of Fluidization and Fluid-particle Systems, Marcel Dekker, Inc., New York, USA. 2003

[3] J.F. Davidson, R. Clift and D. Harrison, Fluidization, Academic Press, London, UK. 1985

[4] D. Kunii and O. Levenspiel, Industrial & Eng Chem Process Design and Development. 1968,7, 481.

[5] R. Jackson, The Dynamics of Fluidized Particles, Cambridge University Press, Cambridge, UK, 2000

[6] L.S. Fan, and C. Zhu, Principles of Gas-Solid Flows, Cambridge University Press, Cambridge, UK. 1998.

[7] L.G. Gibilaro , Fluidization Dynamics, Butterworth Heinemann, Oxford, UK. 2001

[8] D. Geldart , Gas Fluidization Technology, John Wiley & Sons, New York, USA. 1986

[9] D. Gidaspow , Multiphase Flow and Fluidization: Continuum and Kinetic Theory Descriptions, , Academic Press, San Diego, USA. 1994

[10] G. Hetsroni, Handbook of Multiphase Systems, Hemisphere Publishing Corporation, Washington, USA. 1982

[11] D. Geldart, Powder Tech. 1973, 7, 285.

[12] H.T. Bi, and J.R.Grace, Int. J. Multiphase Flow. 1995, 21, 1229.

[13] J.R. Grace, Contacting modes and behavior classification of gas-solid and other 2-phase suspension, Canadian Journal of Chemical Engineering. 1986, 64, 353.

[14] R.D Toomey, and H.F. Johnstone, Gaseous fluidization of solid particles. Chem Eng Progress. 1952, 48, 220.

[15] N.M.Čatipović, G.N. Jovanovic, T.J. Fitzgerald, T.J. AIChE Journal. 1978, 24; 543.

[16] A. Hunt, Measurement and Control. 2014, 47, 19.

[17]. A. Hunt. 4th European Flow Measurement Workshop, Noordwijk, Netherlands, 29-31 March 2016.

[18]. W.Q. Yang and L. Peng, Meas. Sci. Technol. 2003, 14, R1-R13.

[19]. J.S. Halow, G.E. Fasching, and P. Nicoletti, Chem Eng Sci. 1993, 48, 643.

[20]. J.S. Halow, and P. Nicoletti, Powder Technology. 1992, 69, 255.

[21]. S.J. Wang, T., Dyakowski, C.G. Xie, R.A., Williams, R.A. and M.S. Beck, Chem Eng Journal. 1995, 56, 95.

[22]. B.J. Azzopardi, K., Jackson, J.P., Robinson, R., Kaji, M., Byars, and A. Hunt, A, Chem Eng Sci. 2008, 63, 2548.

[23]. F.T. Kühn, J.C., Schouten, R.F., Mudde, C.M. Van den Bleek, and B. Scarlett, B, Measurement Sci and Tech. 1996, 7, 361.

[24]. I. Sidorenko, and M.J. Rhodes, M.J, Powder Technology. 2004, 141, 137.

[25]. D.J. Holland, Q., Marashdeh, C.R., Müller, F. Wang, J.S. Dennis, L.S. Fan, and L.F. Gladden, Industrial Eng Chem Research. 2009, 48, 172.

[26]. J. Baeyens, and D. Geldart, , Chem Eng Sci. 1974, 29, 255.

[27]. J. Verloop, and P.M. Heertjes P.M, Chem Eng Sci. 1974, 29, 1035.

[28]. C.G.J. Baker and D. Geldart, D, Powder Technology. 1978, 19, 177.

[29]. C.R. Müller, J.F., Davidson, J.S., Dennis, P.S., Fennell, L.F., Gladden, A.N., Hayhurst, M.D. Mantle, A.C. Rees, and A.J. Sederman, Chem Eng Sci. 2007,62, 82.

[30]. C.R. Müller, J.F., Davidson, J.S., Dennis, P.S., Fennell, L.F., Gladden, A.N., Hayhurst, M.D. Mantle, A.C. Rees, and A.J. Sederman , Powder Technology. 2007,177, 87.

[31]. P.S.B. Stewart and J.F. Davidson, J.F, Powder Technology. 1969, 1, 61.

[32]. C.E. Agu, L Tokheim, M Eikeland, B.M.E Moldestad, Chem Eng Journal. 2017, 328, 997.

[33]. N. Hilal, M.T. Ghannam, and M.Z. Anabtawi, Chem Eng and Tech. 2001, 24, 161.

[34]. B.J. Azzopardi, H.K. Do, A. Azzi, V. Hernandez Perez, Exp Ther and Fluid Sci. 2015, 60, 1.

[35] G. Costigan, P. Whalley, Int. J. Multiphase. 1997, 23, 263.

[36]. J.M. Matsen, S. Hovmand, J.F. Davidson, Chem. Eng. Sci. 1969, 24, 1743.

[37]. S.H. Lee, D.H., Lee, S.D., Kim, S.D. (2001), Korean J. Chem. Eng. 2001, 18, 387.